Combust. Sci. and Tech., 179: 617–636, 2007

ISSN: 0010-2202 print/1563-521X online
DOI: 10.1080/00102200600969979

Taylor & Francis
Taylor & Francis Group

REDUCED-ORDER MODELING OF DYNAMIC HEAT RELEASE FOR THERMOACOUSTIC INSTABILITY PREDICTION

XINMING HUANG
WILLIAM T. BAUMANN*

Department of Electrical and Computer Engineering, Virginia Tech, Blacksburg, Virginia, USA

The feedback interaction between dynamic heat release and the acoustic characteristics of a combustor can produce an unstable "self-excited" system that ultimately results in a steady pressure oscillation. A simplified model of this feedback loop is needed to predict the limit cycle frequencies and amplitudes. This paper is focused on the development of a physically-based, reduced-order, nonlinear heat release model for a burner-stabilized, laminar premixed flame in a laboratory combustor. Starting from the governing conservation equations, the heat release dynamics are described by partial differential equations that are simulated by a finite-difference method. Using proper orthogonal decomposition (POD) and a generalized Galerkin procedure, the infinite-dimensional PDE model can be reduced to a set of low-order nonlinear ordinary differential equations. The issues of model order versus accuracy and the selection of mode shapes to be used in the reduction are discussed. In addition, this theoretical model points out some major challenges that need to be faced when trying to identify an accurate nonlinear heat release model from experimental data. A two-mode linear acoustic model for the combustor is coupled to the unsteady heat

Received 22 May 2002; accepted 9 July 2006.

This work was funded in part under subcontracts from SCIES as part of the DOE AGTSR/UTSR programs: Contracts 98-01-SR065 and 02-01-SR099, project manager Dr. Richard Wenglarz.

***Address correspondence to baumann@vt.edu**

release model and the resulting closed-loop response is compared to experimental data.

Keywords: heat release dynamics, reduced-order model, thermoacoustic instability

INTRODUCTION

The subject of thermoacoustic instabilities has received significant attention recently because of a move to lean premixed combustion in gas turbines as a means of reducing emissions. The prediction of the exact conditions for which instabilities will occur is very difficult, even for the simplest cases, due in part to the lack of simple models of the dynamics of heat release. Although the steady heat release rate is well understood as a function of operating conditions, the dynamics of the heat release rate in response to perturbations in incoming mass flow or equivalence ratio has not received much attention, either experimentally or with regard to low-order modeling.

In this paper we look at the simple case of a laminar flame in a tube combustor. For this situation, the instability mechanism is well known and can be diagrammed as in Figure 1. A variation in the acoustic particle velocity causes a change in the mass flow of reactants into the flame. This causes a change in the heat release rate that in turn forces the acoustics, creating a physical feedback loop that can go unstable. Our interest is in generating linear and nonlinear reduced-order models of the heat release dynamics from simplified first-principles equations in

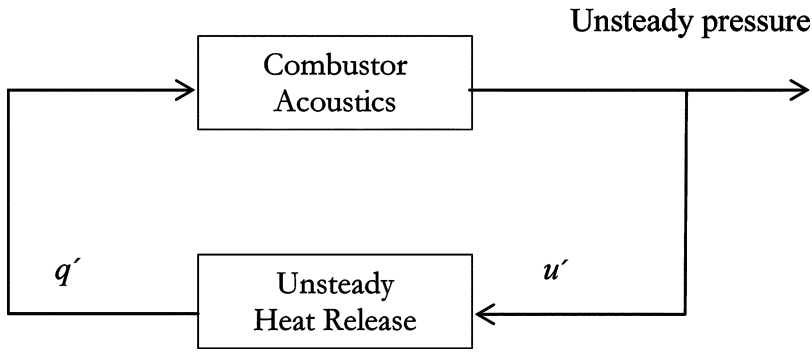

Figure 1. A feedback structure for thermoacoustic instabilities.

order to understand the required complexity of such models for the prediction of limit-cycle frequencies and amplitudes. The implications of these results for low-order modeling and the identification of the heat release dynamics from experimental measurements will also be addressed.

PHYSICALLY BASED HEAT RELEASE MODEL

The development of our physically based model begins with simplified equations governing a one-dimensional laminar premixed flame. A single-step global-reaction mechanism for methane-air combustion is considered.

$$CH_4 + 2(O_2 + 3.76\,N_2) = CO_2 + 2H_2O + 7.52\,N_2$$

Assuming that the fuel is the limiting species and the equivalence ratio $\phi < 1$, the relevant equations are (Margolis, 1980):

$$\frac{\partial Y}{\partial t} + m_0 \frac{\partial Y}{\partial \psi} = \rho^2 D \frac{\partial^2 Y}{\partial \psi^2} - \rho^{-1} RM \tag{1}$$

$$\frac{\partial T}{\partial t} + m_0 \frac{\partial T}{\partial \psi} = \frac{\rho\lambda}{c_p} \frac{\partial^2 T}{\partial \psi^2} + \frac{RM}{\rho c_p} (h_r^o - h_p^o) \tag{2}$$

where T is the temperature, Y is the mass fraction of the fuel and R is the rate term in Arrhenius form (Turns, 1996)

$$R = \upsilon_f k \rho^{\upsilon_f + \upsilon_o} M_o^{-\upsilon_o} M_f^{-\upsilon_f} Y_o^{\upsilon_o} Y_f^{\upsilon_f} e^{-E/RT} \tag{3}$$

where Y_f and Y_o are the mass fractions of the fuel and oxidizer, M_f and M_o are molecular weights, υ_f and υ_o are the corresponding stoichiometric coefficients, and k is the pre-exponential constant. It is also assumed that c_p, $\rho\lambda$, and $\rho^2 D$ are constant and equal for all species (Margolis, 1978). Although these assumptions could be relaxed, given the numerical nature of our scheme, they considerably simplify the equations. One consequence is that the equations for the different mass fractions are not independent and only the fuel mass fraction must be tracked. The mass fraction for O_2 is computed from the fuel mass fraction using

$$Y'_{o_2} = Y'_{CH_4} \frac{M_{O_2}}{M_{CH_4}} \frac{\nu_{O_2}}{\nu_{CH_4}} \tag{4}$$

where a variable with superscript prime represents a variation from the steady-state value. In addition, the ψ streamline coordinate is used instead of x, where (Margolis, 1978)

$$\psi(x,t) = \int_0^x \rho(x,t)dx \tag{5}$$

because it simplifies the equations and also because it causes the input to the flame model, the incoming mass flow rate, $m_0 = \rho u|_{x=0}$, to be an explicit part of the equations. This formulation, in terms of a mass-weighted coordinate, is restricted to 1-D and therefore limits this approach to planar flames. Furthermore, it should be noted that if thermal-diffusive or hydrodynamic instabilities are present in the flame, the assumption of a quasi-steady, planar flame may not be valid.

The output of the system is the rate of heat release to the fluid, which is given by

$$Q_{fluid} = \int_0^\infty R\Delta H_{reac}\ \rho d\psi - \rho\lambda \left.\frac{\partial T}{\partial \psi}\right|_{\psi=0} \tag{6}$$

where ΔH_{reac} is the heat of reaction per unit mass of the mixture. In Eq. (6), the first term represents the heat produced by reaction and the second term denotes heat loss to the burner through conduction. To determine the boundary conditions, we assume that the incoming mixture is at the (constant) burner temperature and that at the end of the reaction zone T and Y reach steady values. The initial mass fraction at $\psi = 0$ is computed according to Fick's law (Turns, 1996). Thus, the relevant boundary conditions are:

$$Y|_{-\infty} = Y|_0 - \left.\frac{\rho^2 D}{m_0}\frac{\partial Y}{\partial \psi}\right|_0 \tag{7}$$

$$T|_0 = T_{burner} \tag{8}$$

$$\left.\frac{\partial T}{\partial \psi}\right|_\infty = 0 \tag{9}$$

$$\left.\frac{\partial Y}{\partial \psi}\right|_\infty = 0 \tag{10}$$

The steady state solution for the profiles, Y° and T°, is obtained by solving Eqs. (1–2) subject to the above boundary conditions using a

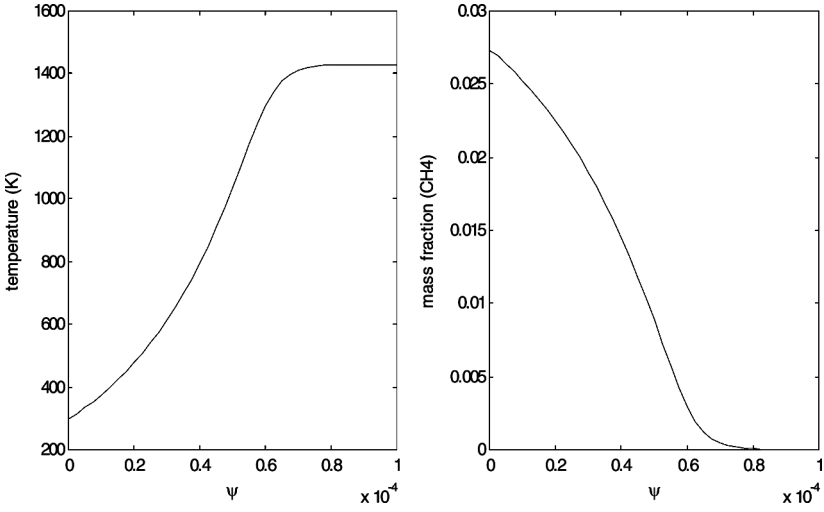

Figure 2. Steady-state temperature and species profiles.

shooting method. A sample steady-state solution is shown in Figure 2 using the following conditions: incoming mixture flow velocity $u_0 = 6\,\mathrm{cm/s}$, burner temperature $T_{\mathrm{burner}} = 300\,\mathrm{K}$, specific heat $c_p = 1.094\,\mathrm{J/g\text{-}K}$, heat conductivity $\lambda_0 = 2.64 \times 10^{-4}\,\mathrm{J/cm\text{-}K\text{-}s}$, thermal diffusivity $D_0 = 0.210\,\mathrm{cm^2/s}$ and Lewis number equal to 1.

SIMULATION USING A FINITE-DIFFERENCE METHOD

To simulate the dynamic response of the flame, the Lagrangian coordinate variable ψ is discretized into a number of equal distance locations, replacing the continuous problem domain by a finite-difference mesh or grid (Kuo, 1986). The number of points n must be selected to guarantee consistence and convergence. With consideration of the two point boundary values, the original partial differential equations (PDEs) are converted into a set of $(n - 2)$ ordinary differential equations (ODEs). Integrating these ODEs approximates the exact solution of the original PDEs. First and second spatial derivatives are obtained by a central difference approximation.

Starting the integration from the nominal steady-state solutions, we obtain the dynamic response of the system. Further grid refinement proves the consistency of the finite-difference approximation. The

number of grid points was chosen to ensure that the truncation error was small. A total of 82 points was applied, generating a system with 80 ordinary differential equations. A time step of 10^{-4} seconds was used. Perturbing the incoming flow velocity about the nominal, $u = u^0 + u'$, results in perturbations of the temperature and species profiles, $T(u', t)$ and $Y(u', t)$, which can be expressed as:

$$T(u', t) = T^0 + T'(u', t) \tag{11}$$

$$Y'(u', t) = Y^0 + Y'(u', t) \tag{12}$$

Various simulations can be set up for different initial conditions and different inputs. The heat release rate can be calculated from Eq. (6). The input of the nonlinear heat release model is the variation of incoming mixture flow velocity u' and the output is the heat release rate per unit area q'. This high-order simulation reproduces the dynamic response of the PDE model accurately, but requires a very high computational load. Thus, we are led to examine the question of how much the order of the model can be reduced while still capturing the relevant dynamics of the heat release system.

MODEL REDUCTION BY PROPER ORTHOGONAL DECOMPOSITION

The simplest way to reduce a system of PDEs to a low-order system of ODEs is to assume that the state of the system can be represented by a finite linear combination of basis functions, or mode shapes, at every instant of time. The coefficient of each basis element in the linear combination is then described by an ODE. The key problem is choosing a basis that will have the lowest number of elements and yet reproduce the system dynamics accurately. The proper orthogonal decomposition (POD) method, also known as the Karhunen–Loeve method, uses the results of high-order time-domain simulations to choose the spatial modes $\phi_i(\psi), i = 0, 1, \ldots, n$ that are most effective in minimizing the error in representing the simulation results (Berkooz et al., 1993; Graham and Kevrekidis, 1996; Park and Cho, 1996; Sirovich, 1986). Mathematically, the problem reduces to an eigenvalue problem for an associated projection matrix, where the eigenvectors are the basis functions and the eigenvalues represent the energy extracted from the data by the associated eigenvector.

Reduced-order modeling, by its nature, must ignore those dynamics of a system that are not important to the analysis being conducted and retain those dynamics that are important. For the thermoacoustic limit-cycle analysis that is our goal, both analysis of the tube combustor and experiments show that the second acoustic mode, which is near 178 Hz, will become unstable in the closed-loop system. Thus, the initial task is to construct a low-order heat-release model that will accurately capture the response to sinusoidal inputs near 178 Hz with a range of amplitudes.

Given an input sinusoid at 178 Hz with various amplitudes between 1 cm/s and 20 cm/s, the finite-difference model simulation gives time-dependent temperature and species mass fraction profiles. We implement the order reduction procedures in deviation variables, that is, the steady-state temperature and species profiles are subtracted from time-dependent temperature and species data and the resulting vector $[T', Y']$ at each timestep is considered as a "snapshot." The integration time lasts 1 second so that the steady-state response is captured, along with the transient. With a sample rate of 20 KHz, 20,000 snapshots are taken for each amplitude value. Combining all of the snapshots corresponding to different input amplitudes, the projection matrix is constructed and the eigenvalue problem is solved using the singular value decomposition (SVD) method.

A number of considerations should be borne in mind to enable accurate approximation. The time-dependent temperature and species data can be represented as,

$$[T'(\psi, t) \quad Y'(\psi, t)]^T = \sum_{i=1}^{N} a_i(t)\phi_i(\psi) \tag{13}$$

where T' and Y' are correlated by the original two partial differential equations (1–2) and the Arrhenius rate Eq. (3). T' and Y' should be treated together, not separately, while doing the modal decomposition. Furthermore, the value of the temperature variation, T', is much bigger than the species mass fraction changes, Y'. Therefore, direct implementation of POD with each snapshot in the form of Eq. (13) actually puts more emphasis on temperature data than species data, since mean square error (MSE) is being minimized. With only a few dominant modal functions, the resulting basis reproduced temperature profiles accurately, but introduced significant errors in the species data. Even though the

Table 1. Energy distribution percentage for first 10 modes

Mode number	Contains energy (%)
1	92.643
2	4.3958
3	2.2217
4	0.54678
5	0.098921
6	0.036595
7	0.033565
8	0.012698
9	0.0069274
10	0.0018313

absolute error of the species data was small, further investigation showed that a small error in mass fraction could lead to a large error in heat-release output due to the Arrhenius term in Eq. (3). We suggest normalization of the snapshot data to balance the energy of T' and Y' before proceeding with the decomposition. For simplicity, a scaling factor $k = 10^5$ was added, so the snapshot becomes $[T'(\psi, t)/k \quad Y'(\psi, t)]^T$.

Table 1 lists the percentage of energy for each dominant mode. The first 10 modes can capture 99.998% of the energy of the snapshots.

After selecting the number of modes to be retained, a Galerkin procedure was applied to obtain a low-order heat release model, consisting of ordinary differential equations for the coefficients $a_1, a_2, \ldots, a_N$.

$$\begin{bmatrix} \dot{a}_1 \\ \dot{a}_2 \\ \vdots \\ \dot{a}_N \end{bmatrix} = \begin{bmatrix} f_1(a_1, a_2, \ldots, a_N, u) \\ f_2(a_1, a_2, \ldots, a_N, u) \\ \vdots \\ f_N(a_1, a_2, \ldots, a_N, u) \end{bmatrix} \tag{14}$$

The output heat release can be computed from Eq. (6), which in the new basis can be represented as,

$$q = g(T, Y) = g(a_1, a_2, \ldots, a_N) \tag{15}$$

Our modeling task is to construct a reduced-order flame model that can accurately reproduce output amplitude and phase due to sinusoidal inputs near 178 Hz. From an energy point of view, it appears we could keep the first 2 modes and do well. If we only consider the small-amplitude inputs, a two-mode approximation works well and accurately

captures the small signal behavior, but has large errors for large-amplitude inputs. Similarly, if we only consider the large-amplitude inputs, a two-mode approximation works well, but has large errors for small-amplitude inputs and does not accurately characterize the linearization of the nonlinear system. As can be seen in Figure 3, the mode

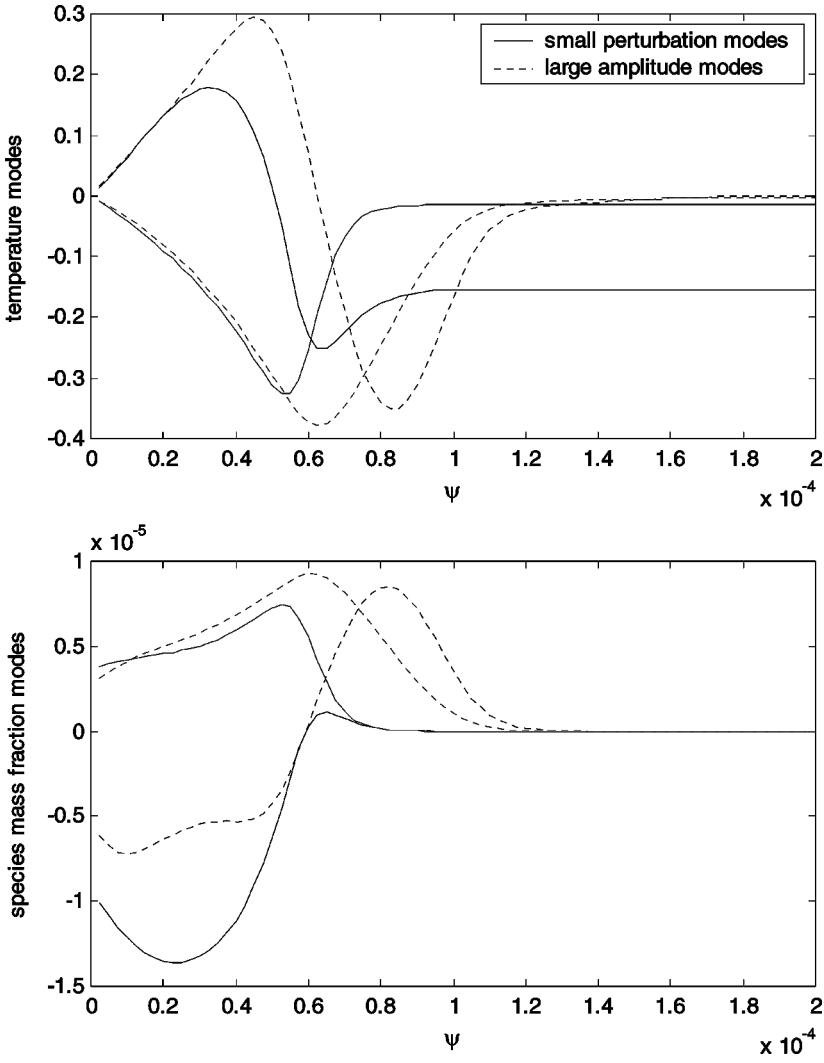

Figure 3. Comparison of modal functions for small and large perturbations.

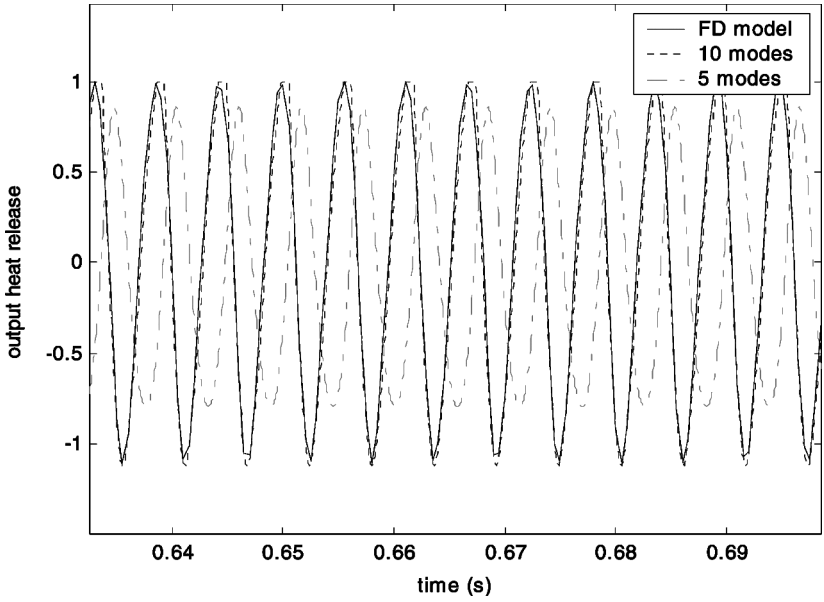

Figure 4. Time domain comparison for input at 178 Hz and amplitude 5 c/s.

shapes for the two cases are significantly different, reflecting the difference in the size of the reaction zone perturbations for the two cases.

To demonstrate the effect of the number of modal functions employed in the POD-Galerkin procedures when the entire data set is considered, the reduced-order nonlinear flame model was simulated by integration of Eqs. (14 and 15) with an input velocity at frequency 178 Hz. Figure 4 shows an example comparison in the time domain (input amplitude 5 cm/s) indicating that the output heat release of a 10-mode model matches the original finite difference output data well, while a 5-mode model shows significant error both in output amplitude and phase. The dynamic model with only 5 modes does not have a sufficient number of basis functions to accurately reproduce the heat release from the complicated reaction terms. Even though the first 5 modes can account for 99.9% of the snapshot energy, there are large errors.

A flat flame burner experiment was used to measure the heat release dynamics due to velocity perturbations (Khanna et al., 2001). With small excitations to acoustic velocity sweeping frequencies from 20 Hz to 400 Hz, the frequency response of the heat release was measured and

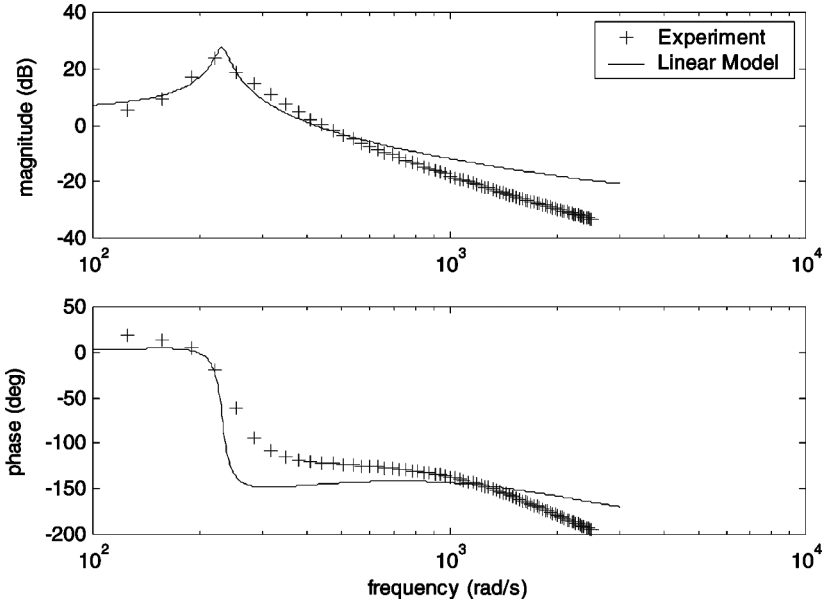

Figure 5. Comparison of linear flame model with experimentally measured frequency response function.

is shown in Figure 5. Two pressure transducers are placed just below the flame holder to measure the acoustic velocity u and a PMT sensor is placed above the flame to measure the OH^* signal, which is assumed to be proportional to the heat release rate q. The peak magnitude of the OH^* signal is then adjusted to match the peak magnitude of the linearized model shown in Figure 5. Compared to the theoretical linear model that we obtained by linearizing the 10th-order nonlinear model, the experimental measurements show basic similarities both in gain and phase response. The linear model we developed is approximately second order. However, the experimental data suggests the linear response is 4th order, which introduces a faster gain and phase roll-off rate. Considering the many physical assumptions and simplifications used in the modeling process, the agreement is quite good.

For limit cycle analysis, it is important that the reduced-order model accurately reproduce the variation in output amplitude as a function of input amplitude. Since the model is nonlinear, output heat release not only contains the fundamental frequency at 178 Hz but also harmonics,

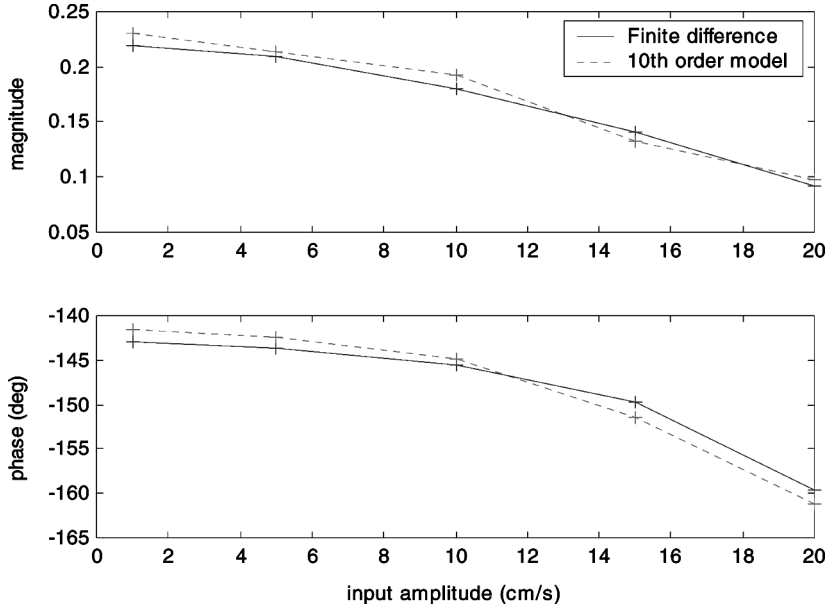

Figure 6. Describing function comparison between 10th-order model and finite difference model at 178 Hz.

which are relatively small. We are only interested in the fundamental output, because eventually the harmonic components will be filtered out by the system acoustic model. A fast Fourier transform (FFT) was performed to obtain the fundamental output magnitude and phase for each simulation run. Figure 6 compares the amplitude and phase of the fundamental component of the 10th-order nonlinear model with the original finite difference model at 178 Hz and demonstrates a reasonable agreement in both magnitudes and phases. Furthermore, the 10th-order nonlinear model also captures these characteristics accurately within the 160 Hz–200 Hz range (results for 200 Hz are shown in Figure 7).

MODELING OF THE CLOSED-LOOP SYSTEM

Thermoacoustic instability arises from the coupling of flame dynamics and acoustic dynamics. One of the important goals of building a reduced-order flame model is to predict the occurrence, frequency and amplitude of the thermoacoustic limit cycle. Here, we make the reasonable assumption that

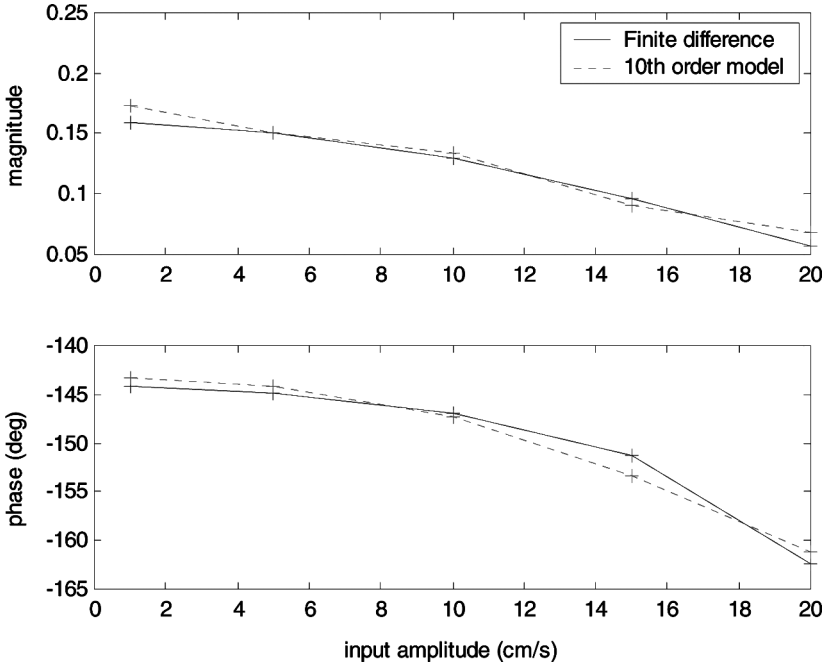

Figure 7. Describing function comparison between 10th-order model and finite difference model at 200 Hz.

the acoustic model is purely linear and only the flame dynamics contain nonlinearity. The parameters used in the system model will be chosen to represent a simple tube combustor for which we have extensive experimental data. The tube combustor is a 60-inch-long steel tube perpendicular to the ground with the top end open and the bottom end acoustically closed. A premixed laminar flame sits on a ceramic honeycomb surface 2.85 inches in diameter located 30 inches from the bottom of the tube (Fannin et al., 1999).

To perform a linear stability analysis of the system, a linear flame model is obtained by linearizing the 10th-order nonlinear model and reducing it to a 2nd-order model using balanced model reduction techniques. The combustor acoustics model can be constructed from simplified conservation equations. Since the flame zone is thin compared to the dimensions of the combustor, we can approximate the reaction spatially as a Dirac delta function. Hence our analysis is restricted to acoustic

wavelengths much larger than the flame thickness. Starting with a one-dimensional model comprising the mass, energy and linear momentum conservation equations (Culick, 1973, 1976), and ignoring the body force, viscosity, and mean flow allows us to write a 1-D wave equation with heat release as a source term (Annaswamy, 1997; Sterling, 1993). Expanding the solution in terms of orthogonal acoustic modes results in

$$p'(x,t) = \sum_{i=1}^{\infty} \psi_i(x)\eta_i(t) \tag{16}$$

$$\ddot{\eta}_i + \omega_i \eta_i = -\bar{\rho}(\gamma - 1)\sqrt{\frac{2}{\bar{\rho}L}}\cos(k_i x_f)\frac{dq'(t)}{dt} \tag{17}$$

$$u'(x,t) = \sum_{i=1}^{\infty} \frac{1}{\gamma k_i^2}\dot{\eta}_i(t)\psi_i'(x) \quad x < x_f \tag{18}$$

where the wave number $k_i = ((2i-1)/2L)\pi$ and the mode function $\psi_i(x) = \sqrt{(2/\bar{\rho}L)}\cos(k_i x)$ (Annaswamy, 1997).

The combustor acoustics model can be constructed from the preceding three equations. The mode numbers can be selected based on the frequency range of interest. Since the linearized flame model shows significant gain only at low frequencies, the combustor acoustic model can be adequately approximated with a few low-frequency modes. The damping of these modes was determined experimentally from measurements on the cold combustor (Huang, 2001).

Table 2 lists the geometry and flow conditions of the laboratory combustor. Using two acoustic modes, the model gives the transfer function, $G(s)$, from the heat release rate changes, $q'(t)$, to the incoming velocity perturbation $u'(t)$, as

Table 2. Summary of the geometry and mean flow of a laboratory combustor

Length of tube combustor	$l = 1.52\,\text{m}$
Flame holder location from closed-end	$x_f = 0.76\,\text{m}$
Diameter of tube combustor	$d = 0.072\,\text{m}$
Flame holder blockage ratio	25%
Damping ratio of 2nd acoustic mode	$\zeta = 1.47\%$
Inlet stagnation temperature	$T_0 = 298\,\text{K}$
Mean density	$\bar{\rho} = 1.21\,\text{kg/m}^3$
Mean pressure	$p = 1\,\text{atm}$

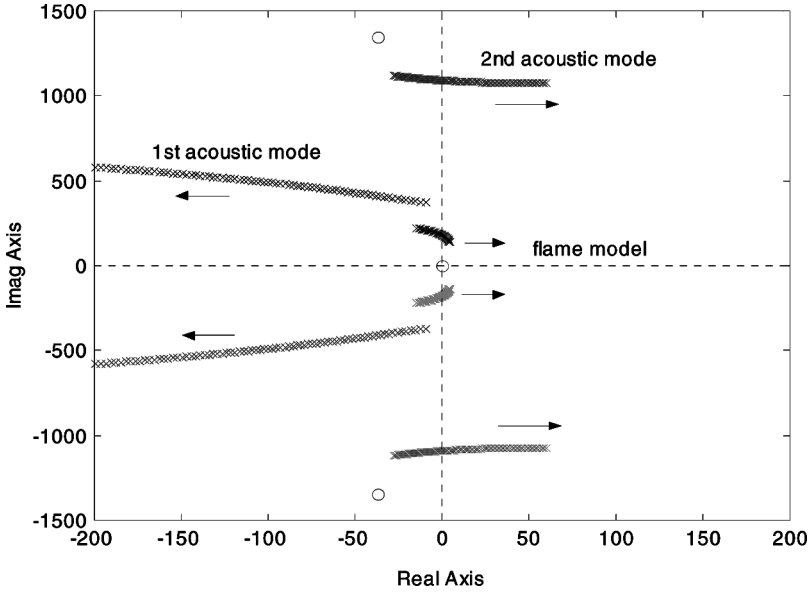

Figure 8. Root locus of the closed-loop linear model.

$$G(s) = \frac{-1.197s^3 - 52.647s^2 - 2165282s}{s^4 + 43.99s^3 + 1393281s^2 + 18367887s + 174331743429}$$

The second-order linear heat release model that we developed earlier has the transfer function,

$$H(s) = \frac{-0.1295s^2 + 193.95s + 93351.43}{s^2 + 29.17s + 48507.80}$$

The root locus technique was applied for the linear system stability analysis and the resulting movement of the closed-loop poles as the system goes from no heat-release feedback (open loop) to full heat-release feedback is shown in Figure 8. The figure clearly demonstrates that the closed-loop system goes unstable. The poles from the first acoustic mode move to the left, which enhances their stability. The second acoustic mode poles move across the imaginary axis near 180 Hz, indicating instability. Meanwhile, the low-frequency poles of the flame model also move into the right half plane for sufficiently high gain, indicating the potential for what is referred to as the thermo-diffusive flame instability.

These results match our experiments in which the instability occurred near 180 Hz in the tube combustor.

Although the response of the unstable linear system will grow without bound, the nonlinearity of the flame model ultimately limits this growth and causes the system to enter into a limit cycle. Linear stability analysis predicts limit cycle frequencies, but the nonlinear reduced-order heat release model is needed to simulate the limit cycle behavior.

With the 10th-order nonlinear flame model coupled to the 4th-order linear acoustic model derived above, the closed-loop system simulation produces a thermoacoustic limit cycle. With conditions, $T_{burner} = 298\,\mathrm{K}$, $\phi = 0.5$ and mean flow of mixture $u_\circ = 6\,\mathrm{cm/s}$, the acoustic pressure oscillation has amplitude 74.7 Pa and the incoming velocity oscillation has amplitude 18.8 cm/s.

With a reference pressure of 20 μPa, the oscillatory acoustic pressure can be converted into a sound pressure level (*SPL*). Figure 9 shows the spectrum of the pressure limit cycle. The acoustic pressure spectrum indicates a peak of 131.4 SPL at a frequency of 178 Hz. Notice that some

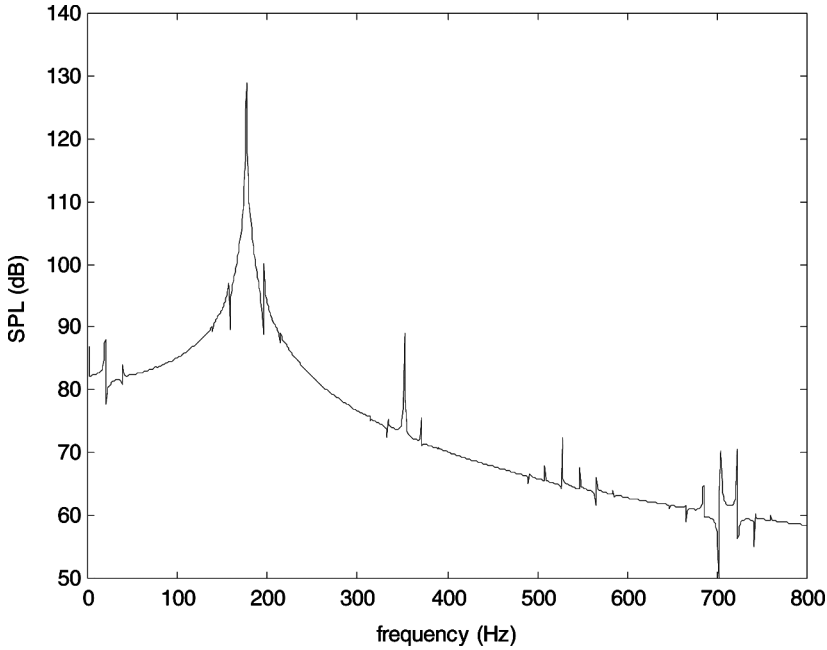

Figure 9. Power spectrum of acoustic pressure limit cycle.

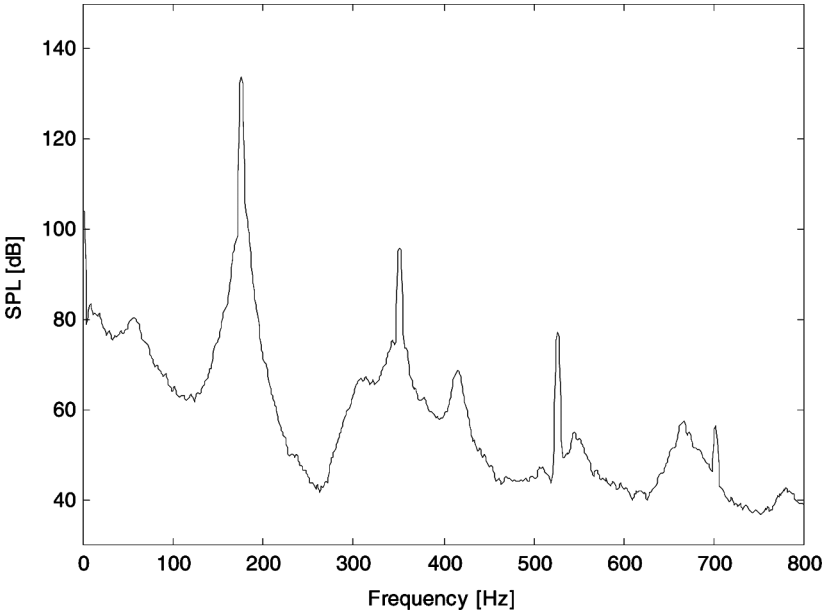

Figure 10. Pressure spectrum for an experimental laboratory combustor.

small side bands start to emerge on the power spectrum of the acoustic pressure limit cycle of the closed-loop nonlinear model simulation. From our linear stability analysis via root locus in Figure 8, there are two low-frequency poles associated with the linear flame model that may be very lightly damped or even slightly unstable. This explains the side band modulation on the pressure spectrum in Figure 9.

In our laboratory tube combustor, experiments with an equivalence ratio of the methane air mixture of $\phi = 0.5$ and a flow rate of 160 cc/s show that a thermoacoustic instability occurs. Figure 10 shows the power spectrum of the pressure measured at the bottom of the tube combustor. The pressure spectrum shows the peak frequency at 178 Hz with an amplitude of 133.7 SPL. Thus, the model is in reasonable agreement with our experimental data.

CHALLENGES TO REDUCED-ORDER MODELING

Although we have produced a reduced-order model capable of capturing the relevant flame characteristics needed to predict limit-cycle frequencies

and amplitudes, this model is actually in the form of an algorithm. Given the coefficients a_i and u, the values of the functions f_i in (14) are solved for by numerically solving the Galerkin equations. Getting a more explicit representation is extremely difficult. Considering the 10th-order model of the form (14–15), each of the functions $f_i(\cdot)$ and $g(\cdot)$ are scalar-valued functions of 11 variables, a_i ($i = 1,\ldots, 10$) and u. If each function is represented by a table and each variable can take m distinct values, then the table will require m^{11} entries. Even for $m = 10$, this amount of data is tremendous.

An alternative is to represent the function by a smaller number of coefficients using a suitable basis $b_i(\cdot)$,

$$f_i(a_1, \ldots, a_{10}, u) = \sum_{i=1}^{N} \alpha_i b_i(a_1, \ldots, a_{10}, u) \tag{19}$$

The question becomes one of choosing a suitable basis. Although this is easy in one dimension, it is very difficult in 11 dimensions. Consider using polynomials. There will be 11 linear terms, 66 quadratic terms, 286 cubic terms, etc. Even if this is a good basis, the number of coefficients that need to be solved for, and the required data, becomes huge. The basis problem can be solved to some extent by using a universal approximator, such as an artificial neural network, but the number of weights and data needed for adequate training are huge.

If it is desired to produce a reduced-order model from experimental data. Not only is a huge amount of data required, but all the states of the system must be measured. This will be incredibly difficult for a 10th-order model and any practical experiment.

CONCLUDING REMARKS

In the previous sections, we proposed a physically-based reduced-order model of a tube combustor. The model consists of a linear acoustic model coupled to a reduced-order model of unsteady heat release with significant nonlinearities. Starting from the governing PDEs, a nonlinear flame model was developed using a POD-Galerkin technique from finite difference simulation data. The metric of success of the 10th-order nonlinear flame model was to reproduce the amplitude and phase of the heat release for sinusoidal inputs near 178 Hz with various amplitudes. As a result, the closed-loop model can successfully predict the thermoacoustic limit cycle frequency and amplitude.

Although the procedure of POD is systematic, the theory does not guarantee the size of an accurate reduced-order model that matches the sought after traits of the original full-order system. To model a complicated system such as a laminar premixed flame, there are significant difficulties in reducing the number of modes. Furthermore, this work points out that there are major difficulties involved in generating an accurate reduced-order model from experimental data.

From the standpoint of control system design, it is possible to predict instability and the resulting limit cycle frequencies and amplitudes using just a linear model and a family of describing functions. The real benefit of a nonlinear dynamic model is simulation. Describing functions only depict steady state characteristics and give no transient information. To see the transient performance of a control system, a dynamic model is required. Furthermore, dynamic simulation is also useful in more complicated situations, such as when there are multiple limit cycles or large random inputs, where analysis becomes very complex.

REFERENCES

Annaswamy, A.M., Fleifi, M., Hathou, J.P., and Ghoniem, A.F. (1997) An input-output model of thermoacoustic instability and active control design. *Report 9705, Dept. of Mechanical Engineering, MIT.*

Berkooz, G., Holmes, P., and Lumley, J.L. (1993) The proper orthogonal decomposition in the analysis of turbulent flows. *Annual Review of Fluid Mechanics*, **25**, 539–575.

Culick, F. (1973) The stability of one-dimensional motions in a rocket motor. *Combust Sci. Technol.*, **7**, 165–175.

Culick, F. (1976) Nonlinear behavior of acoustic waves in combustion chambers-I and II. *Acta Astronautica*, **3**, 715–734, 735–757.

Fannin, C.A., Saunders, W.R., Vaudrey, M.A., Eisenhower, B., and Vandsburger, U. (1999) Analytical and practical considerations for control of thermoacoustic instabilities. *37th AIAA Aerospace Sciences Meeting and Exhibit.*

Graham, M.D. and Kevrekidis, I.G. (1996) Alternative approaches to the Karhunen–Loeve decomposition for model reduction and data analysis. *Computers Chemical Engineering*, **20(5)**, 495–506.

Huang, X. (2001) *Development of Reduced-Order Flame Models for Prediction of Combustion Instability.* Ph.D. Dissertation, Virginia Tech.

Khanna, V., Vansburger, U., Baumann, W.T., Saunders, W.R., and Hendricks, A.D. (2001) *Dynamic Analysis of Burner Stabilized Flames, Part I: Laminar Premixed Flame*, AGTSR annual symposium.

Kuo, K.K. (1986) Principles of Combustion. Wiley, New York.

Margolis, S.B. (1978) Time-dependent solution of a premixed laminar flame. *Journal of Computat. Phys.*, **27**, 410–427.

Margolis, S.B. (1980) Bifurcation phenomena in burner-stabilized flames. *Combustion Sci. Technol.*, **22**, 143–169.

Park, H.M. and Cho, D.H. (1996) The use of the Karhunen–Loeve decomposition for the modeling of distributed parameter systems. *Chem. Eng. Sci.*, **51**(1), 81–98.

Sirovich, L. (1986) Turbulence and the dynamics of coherent structures Part I: Coherent structure. *Quart. Appl. Math.*, **XLV**(3), 561–571.

Sterling, J.D. (1993) Nonlinear analysis and modelling of combustion instabilities in a laboratory combustor. *Combust. Sci. Technol.*, **89**, 167–169.

Turns, S.R. (1996) An Introduction to Combustion: Concept and Applications. McGraw-Hill, New York.